frontiers | Frontiers in Marine Science

TYPE Original Research
PUBLISHED 06 October 2022
DOI 10.3389/fmars.2022.987315



OPEN ACCESS

EDITED BY
Núria Casacuberta,
ETH Zürich, Switzerland

REVIEWED BY
Wei-Koon Lee,
MARA University of Technology, Malaysia
TaeKeun Rho,
Korea Institute of Ocean Science and Technology (KIOST), South Korea

*CORRESPONDENCE
Guebuem Kim
gkim@snu.ac.kr

SPECIALTY SECTION
This article was submitted to Marine Biogeochemistry, a section of the journal Frontiers in Marine Science

RECEIVED 06 July 2022
ACCEPTED 20 September 2022
PUBLISHED 06 October 2022

CITATION
Cho H-M, Han Y, Kim Y-I, Baek C and Kim G (2022) Tracing the depth-dependent changes in organic carbon and nutrient fluxes using high-resolution $^{228}$Ra profiles in the upper East Sea (Japan Sea). *Front. Mar. Sci.* 9:987315. doi: 10.3389/fmars.2022.987315



# Tracing the depth-dependent changes in organic carbon and nutrient fluxes using high-resolution $^{228}$Ra profiles in the upper East Sea (Japan Sea)

Hyung-Mi Cho[1,2], Yongjin Han[1], Young-Il Kim[3], Cheolmin Baek[1] and Guebuem Kim[1]*

[1]School of Earth and Environmental Sciences/RIO, Seoul National University, Seoul, South Korea, [2]Department of Ocean Sciences, Inha University, Incheon, South Korea, [3]East Sea Research Institute, Korea Institute of Ocean Science & Technology, Uljin, South Korea

Vertical profiles of $^{228}$Ra (half-life: 5.75 years) in the ocean provide valuable information on water mixing and ages of the upper ocean. However, its application is hampered by extremely low levels of $^{228}$Ra in the deep ocean. In this study, we measured high-resolution $^{228}$Ra/$^{226}$Ra ratio profiles (>21 depths) in the East Sea (Japan Sea) by mooring Mn-fiber. Using the measured $^{228}$Ra profile from $^{228}$Ra/$^{226}$Ra ratios and $^{226}$Ra activities, together with other previously published data, we estimated the vertical eddy diffusivity (8.7–9.6 cm$^2$ s$^{-1}$) in the permanent thermocline and water ages (10–15 years) in the upper 500–1000 m range. The estimated decomposition rate of organic carbon based on oxygen utilization rates using Ra-ages between 100 and 1000 m was 4.4 ± 0.8 mol C m$^{-2}$ yr$^{-1}$. Our results show that ~50% of the upward nutrients through 100 m support export production, and that dissolved organic carbon accounts for ~20% of carbon export. This $^{228}$Ra approach provides a holistic understanding of carbon and nutrient cycles in the ocean.

KEYWORDS

**Ra-228, Ra-226, nutrients, export production, eddy diffusivity, water age, East Sea**

## Introduction

The vertical water ventilation rate of the ocean thermocline determines the fluxes of nutrients, organic carbon, and other chemical constituents in the ocean. However, it is challenging to determine vertical water mixing rates owing to their dynamic nature, including wind-driven agitation, eddies, fronts, and thermohaline circulation. Thus, geochemists often use tracers to gauge the time-integrated vertical mixing rates in the ocean. The transient tracers for water ages include chlorofluorocarbons (CFCs),

$\delta^3$He-$^3$H, and $^{137}$Cs (Jenkins, 1988; Min and Warner, 2005; Hahm and Kim, 2008; Tsabaris et al., 2020), and the steady-state tracers include cosmogenic $^{14}$C, $^{228}$Ra, and $^{226}$Ra over a basin scale (Moore, 1972; Sarmiento et al., 1976; Moore, 2000; Nozaki and Yamamoto, 2001; Charette et al., 2007).

Transient tracers can be used to determine pathways over a certain period after their arrival in the ocean. Atmospheric concentrations of CFCs began to increase in the 1930s and have decreased since the mid-1990s (Dutay et al., 2002; Bullister, 2015). CFC-11 and CFC-12 enter the surface ocean *via* gas exchange and have been successfully used as time-dependent ocean tracers for the last three decades (Bullister and Weiss, 1983; Warner et al., 1996; Min and Warner, 2005). $^3$H (half-life: 12.3 years) was introduced into the atmosphere from nuclear bomb tests in the 1950s and the 1960s. The $^3$H-$^3$He parent-daughter pair has been applied to estimate water circulation, mixing rates, and water ages (Jenkins, 1977; Jenkins, 1988; Hahm and Kim, 2008). Bomb-produced $^{137}$Cs (half-life: 30.2 years), which peaked during the 1960s, has also been used to trace water mixing (Ito et al., 2003; Tsumune et al., 2003), although it undergoes unknown scavenging, land-based redistribution, and source-input variations. Overall, the use of transient tracers for water-mass mixing rates includes large uncertainties because the time and amount of their inputs to the ocean are not well defined.

Steady-state tracers are not significantly affected by time-dependent variations in source terms; however, their natural source inputs vary significantly over space and time. Their main advantage is the continuous integration of natural processes over a certain period (depending on the half-life of the radionuclides). A cosmogenic nuclide, $^{14}$C (half-life: 5730 years), has been useful in estimating global deep-water ages (Matsumoto, 2007), but its application often includes large uncertainties owing to bomb-produced source inputs. The tracers $^{228}$Ra (half-life: 5.75 years) and $^{226}$Ra (half-life: 1622 years) have been found to be useful for tracing water mixing rates and submarine groundwater discharge over a basin scale (Moore, 2000; Moore, 2003). The main sources of $^{228}$Ra and $^{226}$Ra in the ocean are marine sediments and groundwater (Moore, 1972; Trier et al., 1972; Kaufman et al., 1973; Sarmiento et al., 1976; Sarmiento et al., 1982; Ku and Luo, 1994; Van Beek et al., 2008; Xu et al., 2022). However, the main disadvantage of $^{228}$Ra application in the ocean is that a sample volume of >1000 L for deep water is required to obtain reliable vertical profiles.

Many traditional transient tracers will be phased out in the future; therefore, the use of steady-state tracers will become important for studying oceanic processes. In this study, we attempted to (1) obtain water ages and vertical eddy diffusivities integrated over a period of a decade based on high-resolution $^{228}$Ra profiles obtained using a mooring system and (2) apply such physical information to evaluate oxygen utilization rate (OUR) and decomposition rate of organic carbon, as well as to measure the fluxes of nutrients and dissolved organic carbon (DOC) at depths of 100 m and 200 m. This was performed in the East/Japan Sea (hereafter referred to as the East Sea), which is a semi-closed marginal sea in the northwestern Pacific. It is often regarded as a miniature global ocean because it has its own thermohaline ventilation system with a turnover time of approximately 100 years (Kim et al., 2001).

# Materials and methods

## Study site

The East Sea is a semi-closed marginal sea located in the northwestern Pacific region between the Eurasian continent and Japan. The East Sea consists of three major basins: the Ulleung Basin (UB) in the southwest (>2000 m deep), the Yamato Basin in the south (>2000 m deep), and the Japan Basin in the north (~4000 m deep; Isobe and Isoda, 1997). Water exchange between the East Sea and North Pacific Ocean is limited to the upper layer (~150 m) through four channels: the Korea, Tsugaru, Soya, and Tatar straits (Talley et al., 2003). The temperature of the water masses below approximately 300 m is uniform at 1°C across the entire ocean (Chang et al., 2016). The surface ocean includes various oceanic features, such as subpolar fronts in the central region of the East Sea, warm water in the south, cold water in the north, and numerous eddies (Kim and Legeckis, 1986; Kubota, 1990; Park et al., 2007).

## Sampling and analytical methods

Since the activity of $^{228}$Ra is extremely low in deep-sea water, we determined the ratios of $^{228}$Ra and $^{226}$Ra by mooring $MnO_2$-impregnated fibers (Mn-fibers) at fixed stations where the sediment traps were deployed. Approximately 20 Mn-fibers packed in mesh bags were attached to a wire at each sampling depth (>21 depths). Mn-fiber samples were collected after mooring for 12 days (May 18–29, 2017) at station EC1, 166 days (October 16, 2017 to March 30, 2018) at station EC-trap1, and 164 days (October 17, 2017 to March 29, 2018) at station EC-trap2 in the UB (Figure 1). We neglected any Ra adsorbed onto the Mn-fiber during deployment and retrieval. In addition, samples of approximately 60 L were taken at five depths from mooring station EC1 using a rosette sampler to quantitatively measure $^{226}$Ra activity. The collected seawater sample was gravity-fed through a column of acrylic fiber impregnated with $MnO_2$ at<1 L min$^{-1}$ onboard (Moore, 1976). The activities of $^{228}$Ra were then calculated by multiplying the measured $^{226}$Ra activities by the measured $^{228}$Ra/$^{226}$Ra ratios in the Mn-fiber samples.

The $^{228}$Ra/$^{226}$Ra activity ratios and $^{226}$Ra activities of the samples were measured using a gamma counter. Mn-fiber samples were rinsed gently with distilled water to remove any

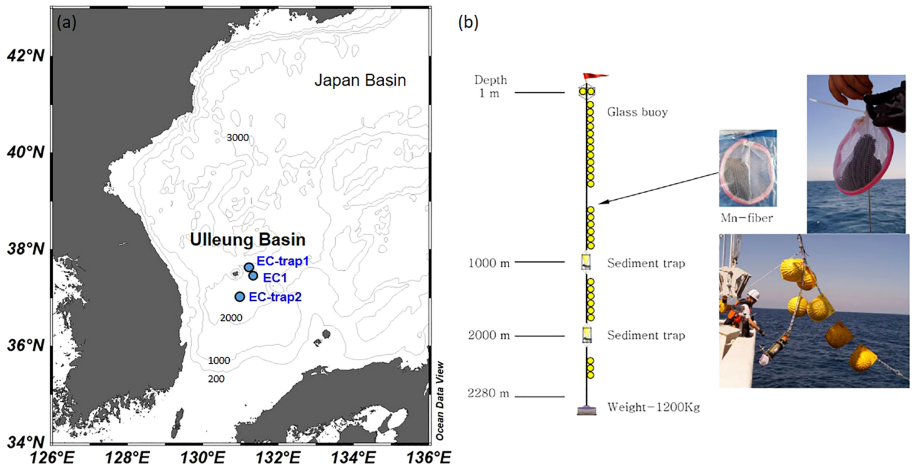


FIGURE 1
**(A)** Geographic locations of Ra mooring stations (blue circle) in the Ulleung Basin (UB) of the East Sea (Japan Sea) in 2017. **(B)** A simplified schematic of the mooring system (left) and photographs of Mn-fiber mesh bags attached to the mooring line (right).

salts, and then the Mn-fibers were ashed at 820°C for 16 h in a muffle furnace and transferred to a sealed vial. The $^{228}$Ra/$^{226}$Ra activity ratios were measured using a high-purity Germanium well-type detector (CANBERRA Industries Inc., Meriden, CT, USA) by counting its daughter nuclide $^{228}$Ac at 911 keV and $^{214}$Pb at 351.9 keV, respectively.

## Calculation of vertical eddy diffusivity based on a $^{228}$Ra profile

If the offshore vertical distribution of $^{228}$Ra is governed by eddy diffusion, a simple one-dimensional diffusion model (Moore, 2000; Charette et al., 2007) can be expressed as

$$\frac{dA}{dt} = K_Z \frac{\partial^2 A}{\partial z^2} - \lambda A \tag{1}$$

where $A$ is the activity of $^{228}$Ra (dpm/100 L), $K_z$ is the vertical eddy diffusion coefficient, $z$ is the depth (m), and $\lambda$ is the decay constant of $^{228}$Ra. In this model, we assume that the only source of Ra is the surface and that the advection or biological effect for Ra is negligible. Assuming a steady-state, Eq. (1) can be written as

$$A_Z = A_0 \cdot exp\left[-z\sqrt{\frac{\lambda}{K_Z}}\right] \tag{2}$$

where $A_Z$ is the Ra activity at a water depth $z$ (m) below the surface. Here, $A_0$ is the Ra activity at a depth of 100 m (bottom of the mixed layer).

If the $^{228}$Ra sources are from both the surface and bottom, although the other assumptions remain the same, the $K_Z$ value can be obtained by applying a two-source diffusion model (Cai et al., 2002). Taking the boundary conditions $A = A_0$ at $z = 0$ and $A = A_L$ at $z = z_L$, the equation can be expressed as

$$\mathrm{Az} = \left(A_L \sinh\left[(\lambda/K_V)^{1/2} z\right]\right) + A_0 \sinh\left[(\lambda/K_V)^{1/2}(z_L - z)\right]\left(\sinh\left[(\lambda/K_V)^{1/2} z_L\right]\right)^{-1} \tag{3}$$

where $\lambda$ is the decay constant of $^{228}$Ra and the boundary value $A_L$ is fixed at depth $z_L$ (2280 m). By fitting the above equation to the vertical profile of $^{228}$Ra with an observed value ($A_L$ = 5.93 dpm/100 L) at 2280 m, we obtain the following equation:

$$\mathrm{A} = (59.3 \sinh(0.002z) + 100.8 \sinh[0.002(2280 - z)])/47.8 \quad (\mathrm{n} = 22,\ \mathrm{R} = 0.96) \tag{4}$$

## Calculation of water ages based on a $^{228}$Ra profile

The decay of $^{228}$Ra can be also used to determine the water mass age at each depth in the upper 1000 m, by assuming the constant initial $^{228}$Ra activity in the surface and downward supply using the equation

$$\left[^{228}Ra\right]_{obs} = \left[^{228}Ra\right]_i e^{-\lambda_{228} t} \tag{Eq.5}$$

where $[228\mathrm{Ra}]_{obs}$ is observed activity of $^{228}$Ra at the sampling depth, $[228\mathrm{Ra}]_i$ is the initial activity of $^{228}$Ra in the surface water, $\lambda_{228}$ is the decay constant for the $^{228}$Ra, and $t$ is the water age. Here, we obtained water ages only for the upper 1000 m where the contribution of bottom sources is relatively small based on the $^{228}$Ra vertical profiles.

# Results

## Vertical profiles of Ra isotopes

Relatively higher $^{228}Ra/^{226}Ra$ activity ratios (~1.0) were observed at the surface and decreased sharply at mid-depths across the thermocline (~0.2 at 500 m), similar to previously published data in the East Sea (Figure 2A). Although the duration and seasons of mooring were different, the $^{228}Ra/^{226}Ra$ profiles at stations EC1, EC-trap1, and EC-trap2 were consistent, indicating the reliability of this approach. In contrast, the $^{228}Ra/^{226}Ra$ activity ratios increased toward the bottom at station EC1, where the sampling approached ~33 m above the bottom (Figure 2A). This trend was not observed at stations EC-trap1 and EC-trap2, where the deepest sampling depths were 260 m and 100 m above the bottom, respectively. The activities of $^{226}Ra$ were lowest (9.7 ± 0.2 dpm/100 L) at the surface and increased by a factor of ~2 with depth (Figure 2B). Such a gradual vertical increase in $^{226}Ra$ is commonly observed in the major oceans (Inoue et al., 2020; Hsieh et al., 2021). The calculated $^{228}Ra$ activities were higher (11 ± 4 dpm/100 L) at the surface and decreased exponentially with depth across the thermocline (Figure 2C and Supplementary Table 1).

## Vertical eddy diffusivity

The observed $^{228}Ra$ data in the East Sea indicate that water mixing in the thermocline is dominated by eddy diffusion, because the plot ($K_Z$) of $ln(A_0/A_z)$ versus depth $z$ (m) is linear (Supplementary Figure 1), as explained by Moore (2000). If only the surface supply of $^{228}Ra$ was assumed, based on Equation (2), the vertical eddy diffusion coefficient ($K_Z$) across 100–400 m in the East Sea was estimated to be approximately 8.7 $cm^2\ s^{-1}$. If the supply of $^{228}Ra$ from the surface and bottom layers is considered, based on Equation (3), the vertical eddy diffusion coefficient ($K_Z$) was estimated to be 8.7–9.6 $cm^2\ s^{-1}$.

The results of the $K_Z$ fitting to the $^{228}Ra$ profiles are shown in Figure 3A. The best-fit curve to the profile ranged between 2 and 14 $cm^2\ s^{-1}$, which agrees with the values obtained using Equations (2) and (3).

# Discussion

## Vertical distribution characteristics of Ra isotopes in the UB

In general, $^{228}Ra$ activity is higher in the surface layer of the global ocean because it is mainly supplied by the continental shelf bottom sediment and the subsequent rapid horizontal mixing (Moore, 1969; Nozaki et al., 1998). In the East Sea, the higher $^{228}Ra$ activity water was mainly from the continental shelf of the Yellow Sea and East China Sea (Cho et al., 2019). Owing to the long water residence times (~5 years) and large shelf dimensions (~1 × $10^6$ $km^2$), these activities are known to be the highest in the world's oceans (40 ± 20 dpm/100 L, Nozaki et al., 1991; Su et al., 2013). An increase in $^{228}Ra$ activity in the bottom layer of the deep ocean has also been observed (~6 dpm/100 L at 2280 m to ~1.6 dpm/100 L at 1500 m) associated with its bottom sediment supply. Moore (1969) showed that the increase in $^{228}Ra$ in the bottom layer is generally observed within 100 m

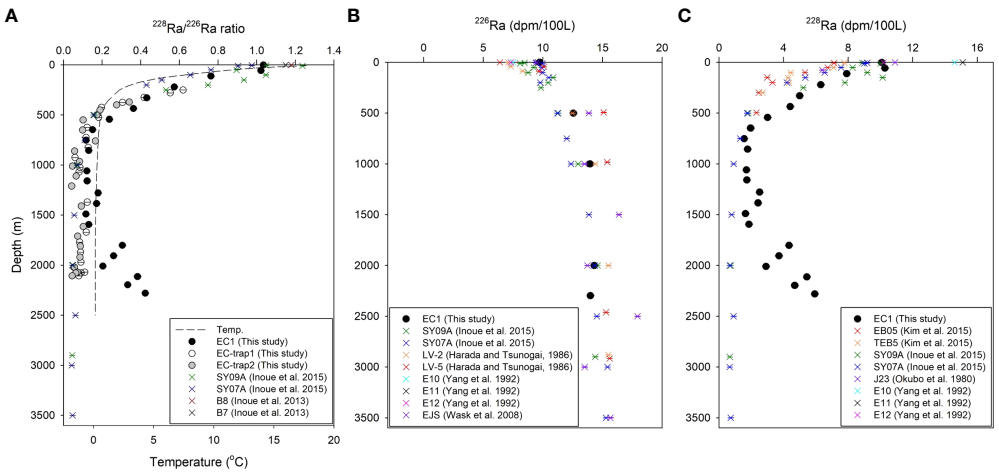


FIGURE 2
Depth profiles of **(A)** 228Ra/226Ra ratios **(B)** $^{226}Ra$, and **(C)** $^{228}Ra$ at stations EC1, EC-trap1, EC-trap2, and other stations from previous studies. The bottom depth at station EC1 is 2313 m.

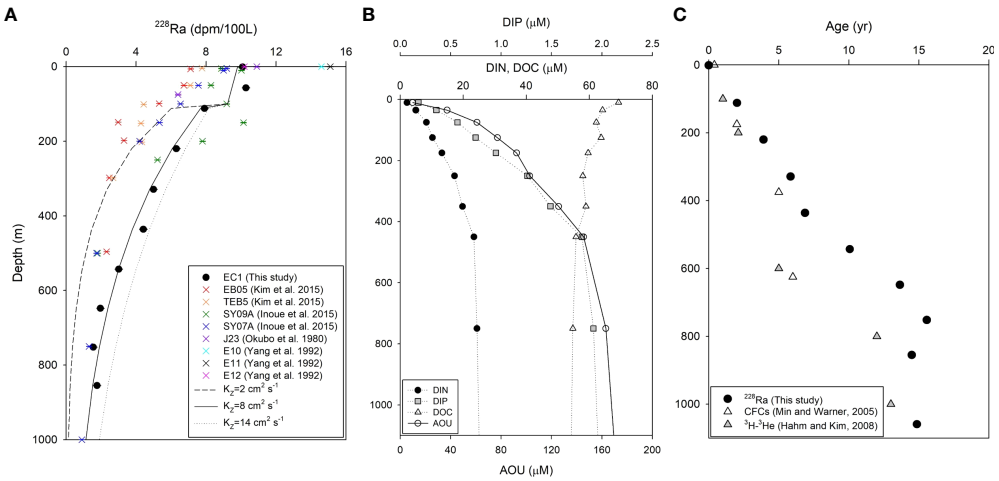


FIGURE 3
**(A)** Model estimates of $K_z$ fitted to the $^{228}$Ra profiles in the Ulleung Basin (UB). **(B)** Vertical profiles of apparent oxygen utilization (AOU), dissolved inorganic nitrogen (DIN) and phosphorus (DIP), and dissolved organic carbon (DOC) from 2006 to 2017 in the UB, East Sea. The dataset is available at the JOISS portal system (http://joiss.kr) which collects and provides marine research data in Korea. **(C)** Comparison of $^{228}$Ra-ages (circles; this study), CFC-11/CFC-12 ratio ages (white triangle; Min and Warner, 2005) in the UB, and $^3$H-$^3$He ages in the Japan Basin (Hahm and Kim, 2008).

from the bottom, which is the benthic boundary layer of the major ocean. This increase is commonly observed in the major oceans (Huh and Ku, 1998; Cai et al., 2002; Charette et al., 2007).

Owing to its relatively long half-life (1622 years), the effect of radioactive decay is negligible in this sea. A constant vertical value from 1000 m to the bottom for $^{226}$Ra was observed (Figure 2B) owing to the well-mixed nature of the deep East Sea (Matsuno et al., 2015). Although there is a significant supply of $^{226}$Ra, together with $^{228}$Ra from the shelf water, it seems to be much smaller than the supply from the bottom of the East Sea.

## Vertical eddy diffusivity in the UB

The vertical eddy diffusion coefficient ($K_Z$) estimated using the $^{228}$Ra tracer, in this study, ranged from 8.7 to 9.6 cm$^2$ s$^{-1}$ in the UB. In the Yamato and Japan basins the vertical eddy diffusivities obtained from $^{236}$U data for six stations varied between 3.4 and 5.6 cm$^2$ s$^{-1}$ (Sakaguchi et al., 2016) in the 150 m bottom depth (>3000 m) layer. As such, the vertical eddy diffusivity determined from the vertical $^{90}$Sr and $^{137}$Cs distributions from the surface to ~2000 m was 4.8 ± 0.7 cm$^2$ s$^{-1}$ (Hirose and Povinec, 2020). The eddy diffusivity from the gradient of the $^{228}$Ra activity around the Yamato Ridge was calculated as ~6 cm$^2$ s$^{-1}$ from the surface to ~1000 m (Tanaka et al., 2006).

The eddy diffusivity in the 100–400 m depth observed in this study was higher than those observed off the coast of Southern California in the equatorial Pacific (1.6 cm$^2$ s$^{-1}$ for the upper 150 m, Knauss et al., 1978), the equatorial Atlantic (0.1 cm$^2$ s$^{-1}$ at 150 m and 0.5 cm$^2$ s$^{-1}$ at 150–225 m, Moore, 1972), and the South China Sea (0.2 cm$^2$ s$^{-1}$ for the upper 300 m, Cai et al., 2002). However, the eddy diffusivity in this sea is one to two orders of magnitude lower than that obtained in the Crozet Plateau region, Southern Ocean (11–100 cm$^2$ s$^{-1}$ in the upper 300 m, Charette et al., 2007) using a 1-D eddy-diffusion-mixing model applied to a $^{228}$Ra profile.

## Vertical exchange of nutrients and DOC

The vertical upward/downward fluxes of nutrients and DOC were calculated by multiplying the calculated eddy diffusivity by nutrient gradients and DOC. In this study, we used datasets for nutrients and DOC in the East Sea from 2006 to 2017. The dataset is available from the JOISS portal system (http://joiss.kr), which collects and provides marine research data in Korea. The concentrations of dissolved inorganic nitrogen (DIN) and phosphorus (DIP) exhibited nutrient depletion at the surface and increased with depth, whereas the vertical trend of DOC was higher in the surface layer than in the deep ocean (Figure 3B). The concentrations of nutrients (DIN and DIP) and DOC showed good negative and positive correlations with $^{228}$Ra activity, respectively, in the 100–400 m layer (Supplementary Figure 2).

The DIN, DIP, and DOC gradients through 100 m (the annual average euphotic zone) were calculated to be approximately 0.06, 0.005, and -0.04 μM m$^{-1}$, respectively. From these gradient values and the calculated vertical eddy diffusivity, we calculated the vertical nutrient and DOC fluxes. The upward fluxes of DIN and DIP at a depth of 100 m were

estimated to be ~1.8 mol N $m^{-2}$ $yr^{-1}$ and ~0.1 mol P $m^{-2}$ $yr^{-1}$, respectively, and the downward flux of DOC was estimated to be ~1.3 mol C $m^{-2}$ $yr^{-1}$. Similarly, the upward fluxes of DIN and DIP at a depth of 200 m were estimated to be ~1.2 mol N $m^{-2}$ $yr^{-1}$ and ~0.1 mol P $m^{-2}$ $yr^{-1}$, respectively, and the downward flux of DOC was estimated to be ~0.6 mol C $m^{-2}$ $yr^{-1}$. The ventilation of water, export production, and the exchange of chemical species in the upper ocean of the East Sea were estimated for a water depth of 200 m in previous studies (Jenkins, 2008; Hahm and Kim, 2008; Kim and Kim, 2013), as the mixed layer in winter often extends to 200 m in the northern part of the sea (Lim et al., 2012). Thus, in this study, for easy comparison with previous studies, we calculated the vertical exchange of nutrients and carbon through 200 m.

## Water ages and oxygen utilization rate

We obtained water ages in the UB of the East Sea using Equation (5) finding that it increased with depth and was approximately 15 years at 800 m (Figure 3C). The age of the oldest water in this study agrees with that estimated using $^{3}H$-$^{3}He$ tracers. However, the ages of the intermediate water mass between 500 and 800 m calculated in this study were much older than those estimated using CFC-11/CFC-12 ratios or $^{3}H$-$^{3}He$ (Figure 3C). This difference could be due to large uncertainties (< 50%) in the CFC ratio age (Min and Warner, 2005) or a more active supply of surface water during the winter of 2000–2001, as suggested by previous studies (Kim et al., 2002; Talley et al., 2003). Yoon et al. (2018) suggested a reduced formation of intermediate water based on the decline in oxygen content.

The OUR in subsurface water between 100 and 1000 m can be determined by the good correlation between the apparent oxygen utilization (AOU) and water age (Figure 4). The AOU is defined as the difference between the oxygen equilibrium value with the atmosphere at the temperature and salinity of the water and the observed oxygen concentration in the same seawater sample. Assuming that the oxygen saturation is almost 100% in the surface water, the integration of OUR in the water column yields a net oxygen consumption of 4.6 ± 1.0 mol $m^{-2}$ $yr^{-1}$ in the layer between 100 and 500 m, and approximately 1.7 ± 0.4 mol $m^{-2}$ $yr^{-1}$ in the layer between 500 and 1000 m based on the slope of AOU versus water ages (Figure 4). The AOU values were calculated based on oxygen, temperature, and salinity data (2006–2017) available on the JOISS portal system (http://joiss.kr).

## OUR and carbon export

The OUR values can be converted to the decomposition rate of organic carbon in the water mass using C:O stoichiometry

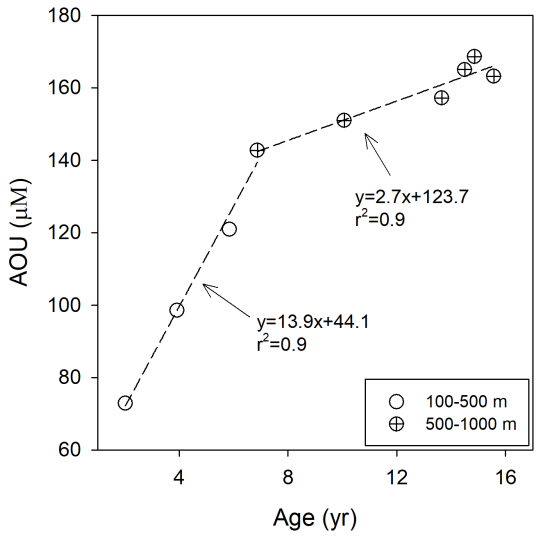


FIGURE 4
Water mass ages versus apparent oxygen utilization (AOU) from 100 to 1000 m in the Ulleung Basin.

(Anderson and Sarmiento, 1994). The estimated decomposition rate of sinking organic carbon in the upper 100–500 m is 3.2 ± 0.7 mol $m^{-2}$ $yr^{-1}$, and 1.2 ± 0.3 mol $m^{-2}$ $yr^{-1}$ at a water depth of 500–1000 m (Figure 5). This result is similar to the estimated export production (~5.3 mol C $m^{-2}$ $yr^{-1}$) in the UB of 200–1600 m by using $^{3}H$ and $^{3}He$ tracers (Kim and Hahm, 2001). Our method showed that ~65% and ~90% of the sinking organic carbon decomposed at depths of 100–500 and 100–1000 m, respectively (Figure 5). Owing to the limitation of age calculation based on $^{228}Ra$, we could not estimate the OUR below 1000 m. Particulate organic carbon (POC) sinking fluxes in the UB at 1000 m were 0–2.6 (0.8 ± 0.5) mol C $m^{-2}$ $yr^{-1}$ based on the sediment trap (Kwak et al., 2017; Kim et al., 2020). Kim et al. (2020) showed that approximately 96% of sinking organic matter is re-mineralized in the upper 1000 m, based on sediment trap studies in this sea. The difference in the DIN fluxes (~0.6 N) between the 100 m (~1.8 N) and 200 m (~1.2 N) depths should be due to the decomposition of DOC and POC fluxes at depth.

According to Kim et al. (2011), POC sinking fluxes in the upper 100 m of the UB were estimated to be 4.9 ± 2.3 mol C $m^{-2}$ $yr^{-1}$ based on measured seasonal variations in $^{234}Th/^{238}U$ disequilibria. As observed in this study, the estimated upward flux of DIN through 100 m supplies approximately 200% of the carbon (DOC + POC) export (Figure 5) based on the Redfield stoichiometry of C:N=106:16. This difference is reasonable because the nutrients that reached the euphotic zone can only be utilized from spring to fall. The estimated downward flux of DOC through 200 m is 50% of that at 100 m. This result shows the effective remineralization of DOC in the subsurface layer as

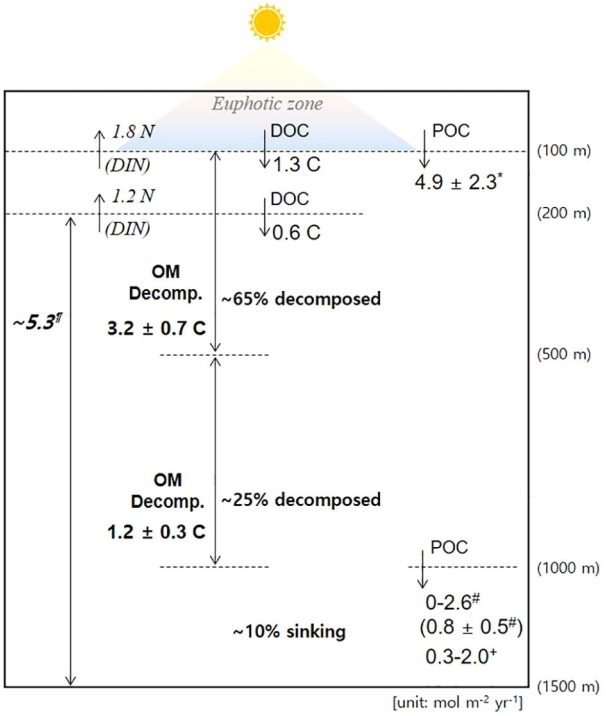


FIGURE 5
A schematic of the vertical fluxes of dissolved inorganic nitrogen (DIN) and organic carbon in the upper East Sea. The vertical fluxes of DIN and dissolved organic carbon (DOC) are based on the DIN and DOC gradients and the estimated eddy diffusivity. OM Decomp. denotes the decomposition rate of organic matter/carbon, which is estimated based on the Ra-age-based oxygen utilization rates (OUR). The downward fluxes of particulate organic carbon (POC) are from previous studies: #Sediment trap (at 1000 m, Kim et al., 2020), +Sediment trap (at 1000 m, Kwak et al., 2017), *234Th method (Kim et al., 2011), and ¶carbon export production using $^{3}$H and $^{3}$He tracers (Kim and Hahm, 2001).

opposed to the unusually slow degradation in the deep layer (Kim et al., 2015). Our results show that DOC accounts for approximately 20% of the total organic carbon export at 100 m (Figure 5), which is lower than that in other regions, including the northern slope of the South China Sea (Zhang et al., 2020), northwestern Sargasso Sea (Carlson et al., 1994), and subtropics (Doval and Hansell, 2000). Kim et al. (2015) showed that DOC in the deep ocean of the East Sea is highly conservative and uniform owing to the lower temperature. Thus, it is likely that POC plays a major role in carbon sequestration in this sea.

## Conclusion

$^{228}$Ra profiles were used to estimate the vertical nutrient and organic carbon fluxes in the UB of the East Sea. The vertical eddy diffusivity ($K_z$) was estimated to be approximately 8.7–9.6 cm$^2$ s$^{-1}$ using one-dimensional diffusion-mixing models of the $^{228}$Ra profiles. By combining the vertical eddy diffusivity with the dissolved nutrients and DOC profiles, we estimated the upward fluxes of DIN and DIP and the downward DOC flux at depths of 100 m and 200 m. In addition, the OUR was estimated by dividing the AOU by the $^{228}$Ra age. Then, the decomposition rates of organic carbon at different water depths (i.e., upper 500 and 1000 m) were obtained using the OUR. These results suggest that high-resolution measurements of vertical $^{228}$Ra profiles are useful for understanding the cycling of carbon and nutrients at different water depths. Our approach can be s similarly applied to other marginal seas and global oceans.

## Data availability statement

The datasets presented in this study can be found in online repositories. The names of the repository/repositories and accession number(s) can be found in the article/ Supplementary Material.

## Author contributions

H-MC and GK wrote the manuscript and analyzed the data. GK contributed to the conception of the study. YH and Y-IK

contributed to sample collection. YH and CB performed the chemical measurements of radium isotopes. All authors contributed to the article and approved the submitted version.

## Funding

This work was supported by the project titled "Deep Water Circulation and Material Cycling in the East Sea (20160400)", funded by the Ministry of Oceans and Fisheries, Korea, and the National Research Foundation (NRF) funded by the Korean government (NRF-2018R1A2B3001147). This research was also supported by the Research Program for the carbon cycle between oceans, land, and atmosphere of the National Research Foundation (NRF) funded by the Ministry of Science and ICT (2022M3I6A1085698). This study was also partially supported by Korea Institute of Marine Science & Technology Promotion(KIMST) funded by the Ministry of Oceans and Fisheries(20220533).

## Conflict of interest

The reviewer TR declared a shared parent affiliation with the author Y-IK to the handling editor at the time of review.

The remaining authors declare that the research was conducted in the absence of any commercial or financial relationships that could be constructed as a potential conflict of interest.

## Publisher's note



## Supplementary material

The Supplementary Material for this article can be found online at: https://www.frontiersin.org/articles/10.3389/fmars.2022.987315/full#supplementary-material

SUPPLEMENTARY FIGURE 1
ln(A0/AZ) values against water depth (m) at the EC1 station, where A0 is the $^{228}$Ra activity at the boundary (100 m depths, bottom of the mixed layer), and AZ is the 228Ra activity water depth z (m).

SUPPLEMENTARY FIGURE 2
Correlations between $^{228}$Ra activities and the concentrations of (a) dissolved inorganic nitrogen (DIN) and phosphorus (DIP) and (b) dissolved organic carbon (DOC) from 100 m to 400 m (the permanent thermocline of the East Sea).

## References

Anderson, L. A., and Sarmiento, J. L. (1994). Redfield ratios of remineralization determined by nutrient data analysis. *Glob. Biogeochem. Cycles* 8 (1), 65–80. doi: 10.1029/93GB03318

Bullister, J. (2015). *Atmospheric histories, (1765–2015) for CFC-11, CFC-12, CFC-113, CCl4, SF6 and N2O, NDP-095* (Oak Ridge, Tennessee: Carbon Dioxide Information Analysis Center, Oak Ridge National Laboratory, US Department of Energy). doi: 10.3334/CDIAC/otg.CFC_ATM_Hist_2015

Bullister, J. L., and Weiss, R. F. (1983). Anthropogenic chlorofluoromethanes in the Greenland and Norwegian seas. *Science* 221, 265–268. doi: 10.1126/science.221.4607.265

Cai, P., Huang, Y., Chen, M., Guo, L., Liu, G., and Qiu, Y. (2002). New production based on $^{228}$Ra-derived nutrient budgets and thorium-estimated POC export at the intercalibration station in the south China Sea. *Deep-Sea Res. I: Oceanogr. Res. Pap.* 49 (1), 53–66. doi: 10.1016/S0967-0637(01)00040-1

Carlson, C. A., Ducklow, H. W., and Michaels, A. F. (1994). Annual flux of dissolved organic carbon from the euphotic zone in the northwestern Sargasso Sea. *Nature* 371 (6496), 405–408. doi: 10.1038/371405a0

Chang, K.-I., Zhang, C.-I., Park, C., Kang, D.-J., Ju, S.-J., Lee, S.-H., et al. (2016). *Oceanography of the East Sea (Japan Sea)* (Switzerland: Springer International Publishing).

Charette, M. A., Gonneea, M. E., Morris, P. J., Statham, P., Fones, G., Planquette, H., et al. (2007). Radium isotopes as tracers of iron sources fueling a southern ocean phytoplankton bloom. *Deep-Sea Res. II: Top. Stud. Oceanogr.* 54, 1989–1998. doi: 10.1016/j.dsr2.2007.06.003

Cho, H.-M., Kim, G., Kwon, E. Y., and Han, Y. (2019). Radium tracing cross-shelf fluxes of nutrients in the northwest pacific ocean. *Geophys. Res. Lett.* 46, 11321–11328. doi: 10.1029/2019GL084594

Doval, M. D., and Hansell, D. A. (2000). Organic carbon and apparent oxygen utilization in the western south pacific and the central Indian oceans. *Mar. Chem.* 68 (3), 249–264. doi: 10.1016/S0304-4203(99)00081-X

Dutay, J. C., Bullister, J. L., Doney, S. C., Orr, J. C., Najjar, R., Caldeira, K., et al. (2002). Evaluation of ocean model ventilation with CFC-11: Comparison of 13 global ocean models. *Ocean Model.* 4 (2), 89–120. doi: 10.1016/S1463-5003(01)00013-0

Hahm, D., and Kim, K. R. (2008). Observation of bottom water renewal and export production in the Japan basin, East Sea using tritium and helium isotopes. *Ocean Sci. J.* 43, 39–48. doi: 10.1007/BF03022430

Hirose, K., and Povinec, P. P. (2020). $^{90}$Sr and $^{137}$Cs as tracers of oceanic eddies in the sea of Japan/East sea. *J. Environ. Radioact* 216, 106179. doi: 10.1016/j.jenvrad.2020.106179

Hsieh, Y. T., Geibert, W., Woodward, E. M. S., Wyatt, N. J., Lohan, M. C., Achterberg, E. P., et al. (2021). Radium-228-derived ocean mixing and trace element inputs in the south Atlantic. *Biogeosciences* 18 (5), 1645–1671. doi: 10.5194/bg-18-1645-2021

Huh, C. A., and Ku, T. L. (1998). A 2–d section of $^{228}$Ra and $^{226}$Ra in the northeast pacific. *Oceanol. Acta* 21 (4), 533–542. doi: 10.1016/S0399-1784(98)80036-4

Inoue, M., Takehara, R., Hanaki, S., Kameyama, H., Nishioka, J., and Nagao, S. (2020). Distributions of radiocesium and radium isotopes in the western Bering Sea in 2018. *Mar. Chem.* 225, 103843. doi: 10.1016/j.marchem.2020.103843

Isobe, A., and Isoda, Y. (1997). Circulation in the Japan basin, the northern part of the Japan Sea. *J. Oceanogr.* 53, 373–382.

Ito, T., Aramaki, T., Kitamura, T., Otosaka, S., Suzuki, T., Togawa, O., et al. (2003). Anthropogenic radionuclides in the Japan Sea: their distributions and transport processes. *J. Environ. Radioact* 68 (3), 249–267. doi: 10.1016/S0265-931X(03)00064-X

Jenkins, W. J. (1977). Tritium-helium dating in the Sargasso Sea: A measurement of oxygen utilization rates. *Science* 196 (4287), 291–292. doi: 10.1126/science.196.4287.291

Jenkins, W. J. (1988). The use of anthropogenic tritium and helium-3 to study subtropical gyre ventilation and circulation. *Philos. Trans. A. Math. Phys. Eng. Sci.* 325 (1583), 43–61. doi: 10.1098/rsta.1988.0041

Jenkins, W. J. (2008). The biogeochemical consequences of changing ventilation in the Japan/East Sea. *Mar. Chem.* 108 (3-4), 137–147. doi: 10.1016/S0265-931X(03)00064-X

Kaufman, A., Trier, R. M., Broecker, W. S., and Feely, H. W. (1973). Distribution of $^{228}$Ra in the world ocean. *J. Geophys. Res.* 78, 8827–8848. doi: 10.1029/JC078i036p08827

Kim, D., Choi, M. S., Oh, H. Y., Song, Y. H., Noh, J. H., and Kim, K. H. (2011). Seasonal export fluxes of particulate organic carbon from $^{234}$Th/$^{238}$U disequilibrium measurements in the ulleung Basin[1] (Tsushima basin) of the East Sea[1] (Sea of Japan). *J. Oceanogr.* 67 (5), 577–588. doi: 10.1007/s10872-011-0058-8

Kim, K. R., and Hahm, D. S. (2001). An estimation of the new production in the southern East Sea using helium isotopes. *J. Korean Soc. Oceanogr.* 36 (1), 19–26.

Kim, T.-H., and Kim, G. (2013). Factors controlling the C:N:P stoichiometry of dissolved organic matter in the n-limited, cyanobacteria-dominated East/Japan Sea. *J. Mar. Syst.* 115-116, 1–9. doi: 10.1016/j.jmarsys.2013.01.002

Kim, M., Kim, Y.-I., Hwang, J., Choi, K. Y., Kim, C. J., Ryu, Y. J., et al. (2020). Influence of sediment resuspension on the biological pump of the southwestern East Sea (Japan Sea). *Front. Earth Sci.* 8. doi: 10.3389/feart.2020.00144

Kim, K. R., Kim, G., Kim, K., Lobanov, V., Ponomarev, V., and Salyuk, A. (2002). A sudden bottom-water formation during the severe winter 2000–2001: The case of the East/Japan Sea. *Geophys. Res. Lett.* 29 (8), 75–71. doi: 10.1029/2001GL014498

Kim, T.-H., Kim, G., Lee, S. A., and Dittmar, T. (2015). Extraordinary slow degradation of dissolved organic carbon (DOC) in a cold marginal sea. *Sci. Rep.* 5 (1), 1–6. doi: 10.1038/srep13808

Kim, K., Kim, K. R., Min, D. H., Volkov, Y., Yoon, J. H., and Takematsu, M. (2001). Warming and structural changes in the East (Japan) Sea: A clue to future changes in global oceans? *Geophys. Res. Lett.* 28 (17), 3293–3296. doi: 10.1029/2001GL013078

Kim, K., and Legeckis, R. (1986). Branching of the tsushima current in 1981–83. *Prog. Oceanogr.* 17 (3-4), 265–276. doi: 10.1016/0079-6611(86)90049-2

Knauss, K. G., Ku, T. L., and Moore, W. S. (1978). Radium and thorium isotopes in the surface waters of the East pacific and coastal southern California. *Earth Planet. Sci. Lett.* 39 (2), 235–249. doi: 10.1016/0012-821X(78)90199-1

Kubota, M. (1990). Variability of the polar front in the Japan Sea. *Sora to Umi* 12, 35–44.

Ku, T. L., and Luo, S. (1994). New appraisal of radium 226 as a large-scale oceanic mixing tracer. *J. Geophys. Res. Oceans* 99 (C5), 10255–10273. doi: 10.1029/94JC00089

Kwak, J. H., Han, E., Hwang, J., Kim, Y. I., Lee, C. I., and Kang, C. K. (2017). Flux and stable c and n isotope composition of sinking particles in the ulleung basin of the East/Japan Sea. *Deep-Sea Res. II: Top. Stud. Oceanogr.* 143, 62–72. doi: 10.1016/j.dsr2.2017.03.014

Lim, S., Jang, C. J., and Park, J. (2012). Climatology of the mixed layer depth in the East/Japan Sea. *J. Mar. Sys* 96, 1–14. doi: 10.1016/j.jmarsys.2012.01.003

Matsumoto, K. (2007). Radiocarbon-based circulation age of the world oceans. *J. Geophys. Res. Oceans* 112, C9004. doi: 10.1029/2007JC004095

Matsuno, T., Endoh, T., Hibiya, T., Senjyu, T., and Watanabe, M. (2015). Formation of the well-mixed homogeneous layer in the bottom water of the Japan Sea. *J. Oceanogr.* 71, 441–447. doi: 10.1007/s10872-015-0303-7

Min, D. H., and Warner, M. J. (2005). Basin-wide circulation and ventilation study in the East Sea (Sea of Japan) using chlorofluorocarbon tracers. *Deep-Sea Res. II: Top. Stud. Oceanogr.* 52, 1580–1616. doi: 10.1016/j.dsr2.2003.11.003

Moore, W. S. (1969). Oceanic concentrations of $^{228}$radium. *Earth Planet. Sci. Lett.* 6, 437–446. doi: 10.1016/0012-821X(69)90113-7

Moore, W. S. (1972). Radium-228: Application to thermocline mixing studies. *Earth Planet. Sci. Lett.* 16, 421–422. doi: 10.1016/0012-821X(72)90161-6

Moore, W. S. (1976). Sampling $^{228}$Ra in the deep ocean. *Deep Sea Res. Oceanogr. Abstr.* 23, 647–651. doi: 10.1016/0011-7471(76)90007-3

Moore, W. S. (2000). Determining coastal mixing rates using radium isotopes. *Cont. Shelf Res.* 20, 1993–2007. doi: 10.1016/S0278-4343(00)00054-6

Moore, W. S. (2003). Sources and fluxes of submarine groundwater discharge delineated by radium isotopes. *Biogeochemistry* 66, 75–93. doi: 10.1023/B:BIOG.0000006065.77764.a0

Nozaki, Y., Dobashi, F., Kato, Y., and Yamamoto, Y. (1998). Distribution of Ra isotopes and the $^{210}$Pb and $^{210}$Po balance in surface seawaters of the mid northern hemisphere. *Deep-Sea Res. I: Oceanogr. Res. Pap.* 45, 1263–1284. doi: 10.1016/S0967-0637(98)00016-8

Nozaki, Y., Tsubota, H., Kasemsupaya, V., Yashima, M., and Naoko, I. (1991). Residence times of surface water and particle-reactive $^{210}$Pb and $^{210}$Po in the East China and yellow seas. *Geochim. Cosmochim. Acta* 55, 1265–1272. doi: 10.1016/0016-7037(91)90305-O

Nozaki, Y., and Yamamoto, Y. (2001). Radium 228 based nitrate fluxes in the eastern Indian ocean and the south China Sea and a silicon-induced "alkalinity pump" hypothesis. *Glob. Biogeochem. Cycles* 15, 555–567. doi: 10.1029/2000GB001309

Park, K. A., Ullman, D. S., Kim, K., Chung, J. Y., and Kim, K. R. (2007). Spatial and temporal variability of satellite-observed subpolar front in the East/Japan Sea. *Deep-Sea Res. I: Oceanogr. Res. Pap.* 54, 453–470. doi: 10.1016/j.dsr.2006.12.010

Sakaguchi, A., Nomura, T., Steier, P., Golser, R., Sasaki, K., Watanabe, T., et al. (2016). Temporal and vertical distributions of anthropogenic $^{236}$U in the Japan Sea using a coral core and seawater samples. *J. Geophys. Research: Oceans* 121, 4–13. doi: 10.1002/2015JC011109

Sarmiento, J. L., Feely, H. W., Moore, W. S., Bainbridge, A. E., and Broecker, W. S. (1976). The relationship between vertical eddy diffusion and buoyancy gradient in the deep sea. *Earth Planet. Sci. Lett.* 32, 357–370. doi: 10.1016/0012-821X(76)90076-5

Sarmiento, J. L., Rooth, C. G. H., and Broecker, W. S. (1982). Radium 228 as a tracer of basin wide processes in the abyssal ocean. *J. Geophys. Res. Oceans* 87, 9694–9698. doi: 10.1029/JC087iC12p09694

Su, N., Du, J., Li, Y., and Zhang, J. (2013). Evaluation of surface water mixing and associated nutrient fluxes in the East China Sea using $^{226}$Ra and $^{228}$Ra. *Mar. Chem.* 156, 108–119. doi: 10.1016/j.marchem.2013.04.009

Talley, L. D., Lobanov, V., Ponomarev, V., Salyuk, A., Tishchenko, P., Zhabin, I., et al. (2003). Deep convection and brine rejection in the Japan Sea. *Geophys. Res. Lett.* 30 (4), 1159. doi: 10.1029/2002GL016451

Tanaka, K., Inoue, M., Komura, K., and Misonoo, J. (2006). Vertical profiles of $^{226}$Ra, $^{228}$Ra and $^{137}$Cs activities in seawater around the yamato ridge and coastal areas of the Sea of Japan. *Chikyu Kagaku* 40, 167–176.

Trier, R. M., Broecker, W. S., and Feely, H. W. (1972). Radium-228 profile at the second GEOSECS intercalibration station 1970, in the north Atlantic. *Earth Planet. Sci. Lett.* 16, 141–145. doi: 10.1016/0012-821X(72)90249-X

Tsabaris, C., Kaberi, H., Pappa, F. K., Leivadaros, P., Delfanti, R., Krasakopoulou, E., et al. (2020). Vertical distribution and temporal trends of $^{137}$Cs at lemnos and Cretan deep basins of the Aegean Sea, Greece. *Deep-Sea Res. II: Top. Stud. Oceanogr.* 171, 104603. doi: 10.1016/j.dsr2.2019.06.011

Tsumune, D., Aoyama, M., and Hirose, K. (2003). Behavior of $^{137}$Cs concentrations in the north pacific in an ocean general circulation model. *J. Geophys. Res. Oceans* 108 (C8), 3262. doi: 10.1029/2002JC001434

Van Beek, P., Bourquin, M., Reyss, J. L., Souhaut, M., Charette, M. A., and Jeandel, C. (2008). Radium isotopes to investigate the water mass pathways on the kerguelen plateau (Southern ocean). *Deep-Sea Res. II: Top. Stud. Oceanogr.* 55, 622–637. doi: 10.1016/j.dsr2.2007.12.025

Warner, M. J., Bullister, J. L., Wisegarver, D. P., Gammon, R. H., and Weiss, R. F. (1996). Basin-wide distributions of chlorofluorocarbons CFC-11 and CFC-12 in the north pacific: 1985–1989. *J. Geophys. Res. Oceans* 101, 20525–20542. doi: 10.1029/96JC01849

Xu, B., Cardenas, M. B., Santos, I. R., Burnett, W. C., Charette, M. A., Rodellas, V., et al. (2022). Closing the global marine $^{226}$Ra budget reveals the biological pump as a dominant removal flux in the upper ocean. *Geophys. Res. Lett.* 49 (12), e2022GL098087. doi: 10.1029/2022GL098087

Yoon, S.-T., Chang, K.-I., Nam, S., Rho, T., Kang, D.-J., Lee, T., et al. (2018). Re-initiation of bottom water formation in the East Sea (Japan Sea) in a warming world. *Sci. Rep.* 8, 1–10. doi: 10.1038/s41598-018-19952-4

Zhang, M., Wu, Y., Wang, F., Xu, D., Liu, S., and Zhou, M. (2020). Hotspot of organic carbon export driven by mesoscale eddies in the slope region of the northern south China sea. *Front. Mar. Sci.* 7. doi: 10.3389/fmars.2020.00444